ChemPubSoc Europe

DOI: 10.1002/batt.201900106

BATTERIES & SUPERCAPS
Articles

Special Collection

Enabling High Performance Potassium-Based Dual-Graphite Battery Cells by Highly Concentrated Electrolytes

Patrick Münster,[a] Andreas Heckmann,[a] Roman Nölle,[a] Martin Winter,[a, b] Kolja Beltrop,*[a] and Tobias Placke*[a]

This work studies an advanced potassium dual-graphite battery (DGB) cell system based on a highly concentrated electrolyte (HCE), *i.e.*, potassium bis(fluorosulfonylimide) (KFSI) in ethyl methyl carbonate (EMC). Structural and electrochemical properties of the designated KFSI/EMC electrolyte are investigated and discussed at different concentrations (1.0 M–4.0 M). Ionic aggregation at high salt concentrations leads to enhanced electrochemical stability and pushes the oxidative stability limit beyond 5 V *vs.* $K|K^+$. Based on those results, the electrochemical performance with graphite as positive and negative electrode active material in graphite||K metal cells is presented. For potassium intercalation into graphite, an impressive capacity retention and rate capability is found for the EC-free HCEs (EC = ethylene carbonate), outperforming potassium electrolytes used in the literature. New insights into the formation of the solid electrolyte interphase (SEI) are presented and confirm improved electrochemical performance. Additionally, high salt concentrations in the electrolyte stabilize the aluminium (Al) current collector and enable reversible intercalation of FSI anions into the graphite positive electrode. Furthermore, reversible cycling in DGB cells is shown and a capacity fading mechanism based on parasitic side reactions causing K^+ ion accumulation in the negative electrode, followed by K metal plating, is comprehensively evaluated.

1. Introduction

Among energy storage technologies, rechargeable batteries offer huge advantages. They combine benefits of high power, and high energy. The extensive versatility offers a broad range of possible applications with respect to different key requirements and represses other energy storage systems to their specific and special fields.[1] Currently, lithium ion batteries (LIBs) are the most prominent battery technology. They are successfully used in small mobile devices such as cell phones for a long time, as well as for large scale-applications such as in electric vehicles.[2,3] Huge advantages are their high gravimetric and volumetric energy density combined with high safety, high reliability, high energy efficiency and high durability compared to other energy storage systems.[4]

A major disadvantage of LIBs on the other hand is the use of non-abundant materials, in particular at the cathode side. Lithium itself occurs in the earth crust with 0.003 wt.%.[5] In addition, mining brings ecological and economic problems. Transition metals such as Co and Ni often used as positive electrode active materials raise similar concerns.[6] They are poisonous and their production is cost- and energy-intensive. Compared to current battery technologies like lithium ion technologies, the use of "greener" materials is favorable, in particular materials or elements which are less toxic, sustainable or having a higher natural abundance and have lower cost are needed. As replacement for lithium, alkali and earth-alkali elements like sodium (Na), potassium (K) and magnesium (Mg) are under consideration for application in sodium-ion batteries (SIBs), potassium-ion batteries (PIBs) and magnesium (ion) batteries.[7] However, all of these elements show a higher redox potential than lithium, i.e., $Mg|Mg^{2+}$: −2.38 V *vs.* standard hydrogen electrode (SHE), $Na|Na^+$: −2.71 V *vs.* SHE and $K|K^+$: −2.94 V *vs.* SHE, compared to $Li|Li^+$: −3.04 V *vs.* SHE. Thus, the batteries are likely to have a lower energy content than LIB. On the other hand, practical electrode potentials show a different behavior in organic solvent-based electrolytes than those calculated as standard potentials for aqueous electrolytes. For instance, in propylene carbonate (PC) K metal plating and stripping may even occur at lower potentials than for Li metal.[8,9] The advantage of the alternatives to Li (Na, K, *etc.*) is their higher abundancy in the earth crust and the seawater, so the production will be easier and less cost intensive,[5] when at the end the achievable energy densities (in Wh/kg or Wh/L) are comparable. If the energy densities of the alternative system are significantly lower than those of LIBs, then this advantage

[a] *P. Münster, Dr. A. Heckmann, R. Nölle, Prof. Dr. M. Winter, Dr. K. Beltrop, Dr. T. Placke*
University of Münster, MEET Battery Research Center
Institute of Physical Chemistry
Corrensstr. 46, 48149 Münster (Germany)
E-mail: tobias.placke@uni-muenster.de
kolja.beltrop@uni-muenster.de
[b] *Prof. Dr. M. Winter*
Helmholtz Institute Münster, IEK-12,
Forschungszentrum Jülich GmbH
Corrensstr. 46, 48149 Münster (Germany)

Supporting information for this article is available on the WWW under https://doi.org/10.1002/batt.201900106

An invited contribution to a Special Collection dedicated to the Symposium on Batteries and Supercapacitors at the E-MRS Spring Meeting 2019

may diminish, as more material, thus more mining effort per Wh/kg or Wh/L is necessary.

Graphite is well known as standard intercalation anode in lithium ion batteries.[10] When graphite is used in rechargeable battery alternatives to Li, potassium is favorable compared to Na or Mg, because it has a high theoretical and practical capacity for the intercalation into graphite (KC_8: 279 mAh g^{-1}) together with a good long-term cycling stability.[11,12]

Next to the substitution of Li, the replacement of less abundant and high cost metals in positive electrode active materials is of great interest. The usage of graphite not only as negative, but also as positive electrode active material generates a so-called dual-carbon battery (DCB) or dual-graphite battery (DGB).[13,14] In combination with suitable electrolytes, this type of battery cell enables not only the small alkali metal cations to intercalate into the negative electrode, but also the larger electrolyte counter anions to intercalate simultaneously into the positive electrode. This cell chemistry has economical, ecological and safety advantages.[15,16,17,18] One major challenge is the still relatively low reversible capacity of the positive electrode gained by anion intercalation into graphite, which also limits the total cell capacity of a DGB cell. Their lower gravimetric and volumetric energy density compared to state-of-the-art LIBs prohibits DGBs from usage in mobile devices,[3,13] while the possibility to use low-cost materials and components (*e.g.* natural graphite, potassium-based electrolyte salts) and low cost electrode processing, also at the positive electrodes, qualifies them as possible stationary energy storage system.[13,16]

DGBs on the basis of potassium ions are recently realized with different sorts of electrolytes, *e.g.* KFSI or KPF_6 salts in ionic liquid or carbonate solvents.[19,20,21] In this work, this approach will be used as starting point and combined with another current research topic, the use of highly concentrated electrolytes (HCE), sometimes also referred to as "super concentrated electrolytes"[22]. Other authors already showed that this electrolyte approach offers different beneficial properties than the commonly used "dilute" electrolytes with typically 1 M (mol L^{-1}) dissolved salt.[22,23,24–29] Even though the ion transport properties like decreased ionic conductivity due to enhanced viscosity are undesirable for the use in battery cells, they show some extraordinary features such as different solution structure[24,30] and stabilized electrode/electrolyte interfaces (*e.g.* improved interphase formation,[31] decreased anodic dissolution of the Al current collector,[32] *etc.*). In case of DGB cells, it also has to be mentioned that high salt concentrations are mandatory to achieve a high energy content, as the electrolyte concentration inevitably contributes to a large extent to the inactive mass and volume of the cell. While the electrolyte ions are essential for the charge/discharge mechanism of a LIB cell, the total amount of solvent should be minimized.[3,13] Further, the electrolyte properties in a DGB cell will periodically change during charge/discharge operation, as cations/anions are removed during charge and released back to the electrolyte during discharge of the cell.

In particular, different solvation structures in the HCEs, with usually $\geq$3 mol L^{-1} salt, lead to formation of a completely different, LiF enriched and more effective solid electrolyte interphase (SEI) at the negative electrode.[24,26,29,31,33] This layer was reported to be more compact, and despite the high resistance of LiF towards Li^+ transport, it contributes less to the overall cell resistance than its analogue in commercial LIBs.[24,34] As a result, ethylene carbonate (EC) as co-solvent may be neglected. Commonly, EC is used for its very well SEI-forming behavior together with its high permittivity and therefore ability to dissolve salts.[35,36] The drawback of EC is its high viscosity together with a melting point of 36 °C. Therefore, HCEs can combine the advantages of EC-free and EC-containing electrolytes. The application of HCEs in lithium-based DGBs has already been reported.[27,37,38]

By following this HCE electrolyte approach, the present work focusses on the development of potassium-based dual-graphite batteries with highly concentrated electrolytes based on potassium bis(fluorosulfonylimide) (KFSI) as active salt. The electrochemical behavior against graphitic electrodes is comprehensively investigated with respect to K^+ and FSI^- anion intercalation in graphite||K metal cells and finally results in a potassium-based graphite||graphite cell. Furthermore, the formation of the SEI layer at the negative graphite electrode is comprehensively investigated, giving new insights in its beneficial impact on cell performance.

2. Results and Discussion

2.1. Electrolyte Selection

In this study, we chose KFSI (1 M) as conducting salt in EMC as single solvent as electrolyte for the DIB and DGB cell investigation. A preliminary study showed, that the EMC/KFSI-based electrolyte shows enhanced capacity retention as well as improved rate capability compared to other common electrolyte mixtures used in literature[20,39,40] with respect to K^+ intercalation into graphite negative electrodes for potassium ion batteries (PIBs). Figure 1 presents the electrochemical performance of graphite negative electrodes in combination with different potassium salt-containing electrolytes. A summary of the electrochemical data is presented in Table S1 in the Supporting Information.

A possible reason for the improved electrochemical performance of the EMC/KFSI-based electrolyte compared to the other electrolyte mixtures is most likely the absence of ethylene carbonate (EC). Most of the electrolytes used for PIB studies reported in literature are based on EC as co-solvent.[20,39,40] EC brings the advantage of a high permittivity,[41] so that otherwise hardly soluble salts, such as KPF_6, can be used. Further, EC is known to form an effective solid electrolyte interphase (SEI) on graphite by reductive decomposition during the first charge/discharge cycles, so that a highly reversible (de-)intercalation of K^+ ions is possible. On the other hand, single solvent EC electrolytes show a higher viscosity and lower ionic conductivity compared to electrolytes using only linear carbonates such as EMC.[41] In addition, it was already shown that the ionic conductivity of highly concentrated EC-free electrolytes is

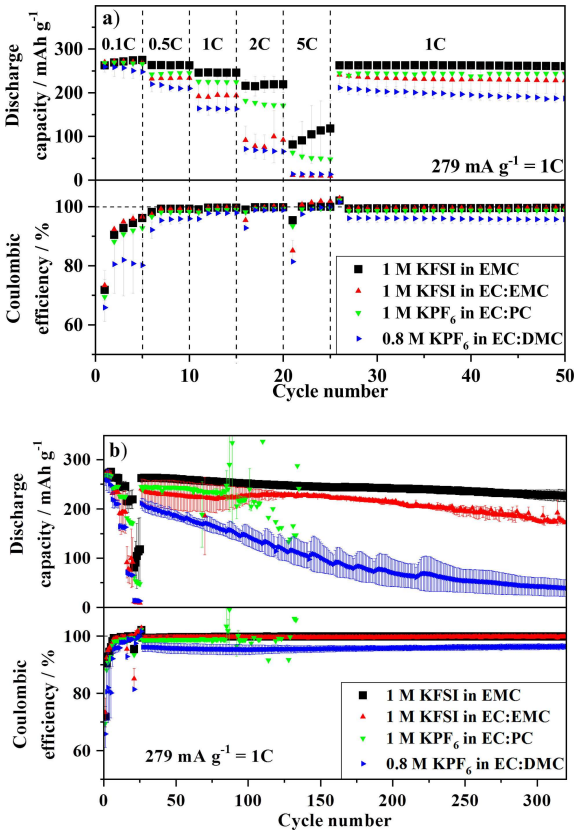

Figure 1. Comparison of specific DC (upper part) and C_{Eff} (lower part) of (a) rate capability and (b) long-term charge/discharge cycling performance for K^+ intercalation/de-intercalation with various electrolytes in a graphite||K metal three electrode cell setup (half-cell setup) with a K metal reference electrode (RE). Cycling was performed between reference-controlled cut-off potentials of 0.02 V and 1.5 V *vs.* K|K^+. The solvent mixtures of EC with EMC, PC or DME were in all cases 1:1 based on volume.[20,39,40]

similar to that of EC-containing electrolyte solutions, despite the higher viscosity of the HCE.[24] To combine the advantages of cyclic and linear carbonates, an appropriate electrolyte salt with good SEI-forming properties can be used. A possibility is KFSI, as the FSI-based electrolytes have a little narrower electrochemical stability window compared to $TFSI^-$ and PF_6^- based salts.[42] However, they also show a decreased protection against anodic dissolution of the Al current collector. Nevertheless, the FSI-salts show excellent dissolution behavior to achieve a high salt concentration, as will be discussed in the next sub-chapter, and have been reported to form a very effective SEI layer.[43,44] On the other hand, high concentrations of KPF_6 and KTFSI in EMC solvent could not be achieved as the salts could not be sufficiently dissolved. Considering all of this, EC as co-solvent may be redundant, when KFSI as salt is used. With this approach, the negative properties of EC, like high viscosity and reduced ionic conductivity, can be excluded and the cell performance can be improved. Based on the results presented here, 1 M KFSI in EMC was used as reference electrolyte for the subsequent studies.

2.2. Ion Environment of KFSI in EMC Studied by Means of Raman Spectroscopy

The specific ion environment inside a salt/solvent mixture, i.e. the solution structure, has a huge impact on the physicochemical properties of the electrolyte[45] and can be determined by means of Raman spectroscopy. Depending on the salt concentration, different interactions of the respected ions with solvent molecules lead to the formation of either solvent separated ion pairs (SSIPs, an anion without direct interaction with K^+), contact ion pairs (CIPs, an anion coordinating to one K^+ ion) or aggregates (AGGs, an anion coordinating to two or more K^+ ions). Therefore, small deviations in the ion-coordination are accompanied with a slight shift in the corresponding Raman signal.[24,29,31] Numerous publications deal with the solution structure of different lithium salts in a variety of protic and aprotic solvents.[22,24–26,46–48] However, the available data on the solution structure for potassium-based electrolytes is still scarce. For example, Xiao et al. showed that there is a shift in Raman signals to higher wavenumbers for higher concentrated KFSI in dimethoxyethane (DME)-based electrolytes due to enhanced interactions with K^+ ions. For the same reason, the CH_2 rocking and C–O stretching modes of the solvent molecule exhibit shifted signals as well.[43]

The results of the Raman spectroscopy measurements of KFSI in EMC at different salt concentrations are depicted in Figure 2.

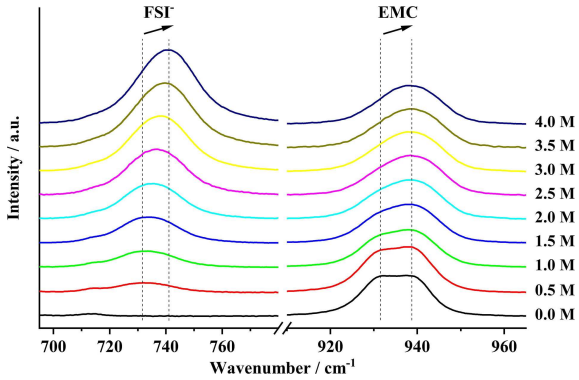

Figure 2. Normalized Raman spectra of dissolved KFSI in EMC at different concentrations from 0.5 M to 4.0 M. The peak at $\tilde{\nu} = 740\ cm^{-1}$ is due to stretching modes from the FSI anion and the one at $\tilde{\nu} = 940\ cm^{-1}$ is created by the solvent EMC. The shifts marked by the included arbitrary lines, symbolize different molecular environments of the respective anion or solvent molecules.

The band at $\tilde{\nu} \approx 740\ cm^{-1}$ is represented by sulfur-nitrogen-sulfur (SNS) stretching modes of the FSI anion.[49] With higher amount of dissolved salt the intensity increases sharply, however, also a shift of the peak maximum can be observed from $\tilde{\nu} = 731\ cm^{-1}$ to $\tilde{\nu} = 744\ cm^{-1}$. This is due to different environments of the investigated anions. In low concentrated solutions, SSIPs are the dominant species, where only negligible interactions between the anion and the corresponding cation are present. With increasing amount of KFSI, and therefore

decreasing amount of EMC, there is not enough solvent left to create a sufficient solvation shell around the anions. As a result, CIPs are formed and, with further addition of the salt, AGGs are generated. SSIPs are thermodynamically favored over CIPs and AGGs in lower concentrated electrolyte solutions, but due to an increase in salt concentration the equilibrium in the system (SSIP⇌CIP⇌AGG) is shifted towards AGGs.

Each of the three different molecular structures exhibits its Raman signal at slightly different wavenumbers.[27,29] A small difference in the electronic structure of the complexes results in slightly different polarizability and therefore a shifted signal. The measured peak at $\tilde{\nu}=740\ cm^{-1}$ is a superposition of different underlying bands for the different solution structures.[29] With a mathematical fit the position of the three bands can be estimated to have values of $\tilde{\nu}=730\ cm^{-1}$ (SSIP), 737 cm^{-1} (CIP) and 744 cm^{-1} (AGG), respectively. The resulting distribution of the fitted bands are presented in Table 1. They stress once more the increased cation-anion interactions when the concentration of the salt is increased.

At $\tilde{\nu}\approx930\ cm^{-1}$, a superposition of different bands is present as well, here representing the C–O stretching mode of the EMC molecule.[50] The uncoordinated and "free" solvent exhibits bands at $\tilde{\nu}=931\ cm^{-1}$ and $\tilde{\nu}=939\ cm^{-1}$ (Figure 2). With increasing salt concentration, the intensity of the latter increases, due to cation complexation by solvent molecules. K^+ is only a weak Lewis acid compared to Li^+ and thus, only a small shift is apparent and the bands for cation-complexation and "free" solvent are overlapping. This is different for lithium-based electrolytes, which can exemplarily be seen by Raman spectroscopic measurements of LiFSI in EMC at different concentrations shown in Figure S1.

The distribution of the fitted bands at $\tilde{\nu}\approx930\ cm^{-1}$ is also shown in Table 1. For concentrations higher than 3.0 M only small changes for the activity of the "free" EMC at $\tilde{\nu}=931\ cm^{-1}$ are visible. It has to be emphasized, that the positions of the different bands were estimated by mathematical fitting and comparison with the corresponding lithium salts.[22,24–26,31,46–48] Therefore, molecular dynamic (MD) simulations and density functional theory calculations have to be performed to further evaluate the results regarding the exact wavenumber for each solution structure. However, results from Ravikumar et al., who calculated proportions of SSIPs, CIPs and AGGs via MD simulations for a system with lithium hexafluorophosphate ($LiPF_6$) in EC as electrolyte, are remarkably similar to the KFSI in EMC electrolyte system.[51] Therefore, the here conducted mathematical fitting can be seen as a valid method to investigate the solution structure of this electrolyte.

2.3. Study of Electrochemical Electrolyte Stability and Aluminium Current Collector Dissolution

The electro(-chemically) induced dissolution of the current collector(s) is a serious threat to the lifetime of rechargeable batteries.[52] With ongoing degradation of the current collector, internal resistances of the cell might increase due to particle loss and decreased structural integrity of the composite electrode. Moreover, further parasitic side reactions can be induced for DGB cells, as it has been reported recently by Heidrich et al.[53] High purity Al foil is the material of choice for an application as current collector for various battery applications (e.g. for the positive electrode in LIBs; for the positive and negative electrode in PIBs; *etc.*), due to its outstanding mix of qualities such as the high electronic conductivity, low material cost and its advantages with respect to its processability to very thin foils ($\leq 10\ \mu m$).[54,55] However, the Al current collector (ACC) tends to show severe dissolution during anodic polarization in several imide-based electrolytes and has been extensively investigated for lithium-salt based electrolytes.[55] In this respect, Meister et al. reported that acidic species, which are be formed by oxidative decomposition of the electrolyte, attack the native oxide layer (Al_2O_3) of the Al foil in the first step, followed by Al dissolution in the second step.[55] No thorough investigation has yet been performed for ACC dissolution in K-imide salt-based electrolyte systems.

The use of huge amounts of salt in the electrolyte should in principle stabilize the current collector sufficiently, as it has been reported for lithium-salt electrolyte systems.[28,55,56] For example, Heckmann et al. showed an improved cycling stability and improved Coulombic efficiency (C_{Eff}) for DGB cells based on highly concentrated lithium-imide (LiTFSI) electrolytes.[27] Therefore, linear sweep voltammetry (LSV) and chronoamperometric (CC) measurements were also conducted for the KFSI-based electrolyte to get a deeper understanding of the performance of the DGB cell setup, which will be discussed below. The oxidative stability of differently concentrated electrolytes

Table 1. Distribution of the band at 740 cm^{-1} on the three underlying bands for SSIPs (730 cm^{-1}), CIPs (737 cm^{-1}) and AGGs (744 cm^{-1}) and distribution of the band at 930 cm^{-1} on the two underlying bands for "free" (931 cm^{-1}) and coordinating (939 cm^{-1}) EMC. The results are calculated based on the Raman spectra shown in Figure 2.

KFSI concentration [mol L^{-1}]	Proportion SSIP [%] (730 cm^{-1})	Proportion CIP [%] (737 cm^{-1})	Proportion AGG [%] (744 cm^{-1})	Proportion free EMC [%] (931 cm^{-1})	Proportion compl. EMC [%] (939 cm^{-1})
0.0	–	–	–	51	49
0.5	88	10	2	46	54
1.0	62	34	4	34	66
1.5	49	48	3	27	73
2.0	31	65	4	19	81
2.5	22	62	16	13	87
3.0	17	57	26	11	89
3.5	15	39	46	10	90
4.0	14	20	66	10	90

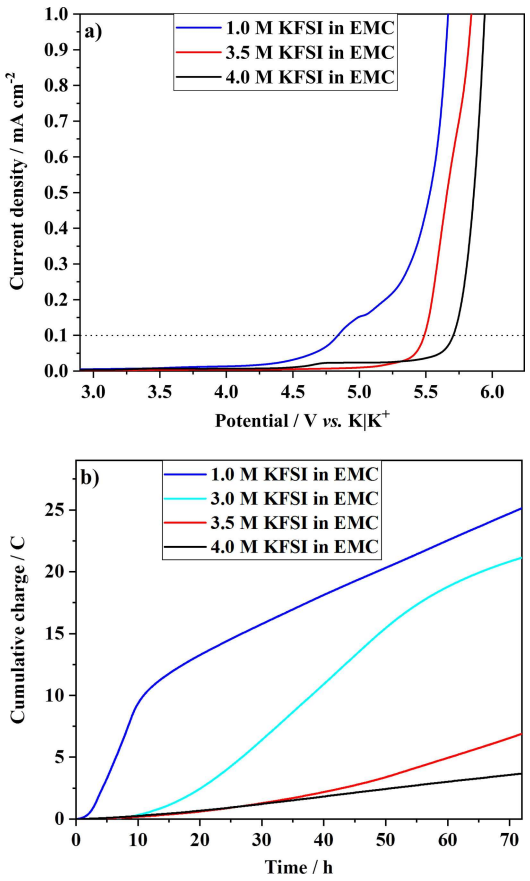

Figure 3. a) Oxidative stability of differently concentrated electrolytes (KFSI in EMC), measured in a Pt| |K metal cell (half-cell setup; K metal RE). The dotted line at an arbitrary defined current density of 0.1 mA cm^{-2} (based on the surface area of the Pt WE) marks the onset potential of the decomposition reaction at a scan rate of 1 mV s^{-1}. b) Cumulative charge due to dissolution of the Al current collector in differently concentrated electrolytes (KFSI in EMC). Measurement was performed in a Al| |K metal cell (half-cell setup; K metal RE). Potential was increased linearly up to 5 V *vs.* K|K$^+$ within 1 h and then held at that potential for 72 h.

(1.0 M—4.0 M) against an inert Pt electrode (working electrode; WE) is depicted in Figure 3a and Table 2.

The LSV measurements show the trend of an increasing oxidative stability with higher KFSI concentration (Figure 3a). The arbitrary defined oxidative stability limit of 0.1 mA cm^{-2} (based on the surface area of the Pt WE) is reached for the electrolyte with 1.0 M KFSI at ≈4.8 V *vs.* K|K$^+$, whereas for the 3.5 M and the 4.0 M electrolyte, the onset potential is shifted up to ≈5.4 V and ≈5.6 V *vs.* K|K$^+$, respectively. The lack of solvent and the according change of molecular solvation structures are responsible for this enhanced electrolyte stability. Interestingly, the oxidative stability limit for the diluted 1.0 M KFSI electrolyte is already relatively high, compared to other electrolytes based on EC as co-solvent.[35] They are comparable with those obtained in systems with ionic liquids (ILs) as solvent[19] or highly concentrated potassium electrolytes with less electrochemically stable solvents, such as DME and propylene carbonate (PC).[57] The reason is the neglection of EC and other (co-)solvents having minor oxidative stabilities. EMC is known to have an increased electrochemical stability.[35]

Table 2. Oxidative stability *vs.* Pt and cumulated charge (taken from chronocoulometry measurements) of differently concentrated electrolytes (KFSI in EMC). The results are obtained from Figure 3a and b.

KFSI concentration in EMC [mol L^{-1}]	Oxidative stability limit at 0.1 mA cm^{-2} [V *vs.* K|K$^+$]	Cumulated charge after 72 h at 5 V *vs.* K|K$^+$ [C]
1.0	4.8	26
3.0	–	21
3.5	5.4	7
4.0	5.6	3

This result in turn offers a variety of possibilities. The diluted KFSI based electrolyte could be used in PIB cells with positive electrode active materials that have a lower operation voltage compared to graphite positive electrodes (≥4.5 V *vs.* K|K$^+$). *Hosaka* et al. recently used "Berlin blue" ($K_2Mn[Fe(CN)_6]$) as positive electrode material in PIB cells, which operates at potentials ≤4.3 V *vs.* K|K$^+$.[57] Similar oxidative stabilities suggest, that the here proposed 1.0 M KFSI in EMC electrolyte could be a low-cost alternative to the 7.0 mol kg^{-1} KFSI in DME, which was used in their work. Recently, similar approaches were published using KFSI in EMC as electrolyte with a carbon negative electrode and different positive electrodes. While a high FSI^- concentration was used to generate a stable potassium ion battery cell based on an organic cathode[58], a lower concentrated 1.0 M KFSI/EMC electrolyte was used with a carbon negative electrode coated with an $MoSe_2$ compound together with a K metal CE and showed excellent rate capability.[59] Overall, it has to be kept in mind that these initial results from LSV measurements on inert Pt electrodes only give a trend for the oxidative electrolyte stability, however, cannot be directly compared to the galvanostatic results, as presented below, where the intercalation and possible decomposition of anions as well as Al current collector dissolution will likely result in increased parasitic currents.

In order to gain a deeper understanding of the compatibility of the investigated electrolytes (1.0 M, 3.0 M, 3.5 M and 4.0 M KFSI in EMC) with the ACC, CC measurements at a potential of 5 V *vs.* K|K$^+$ for 72 h were performed (Figure 3b and Table 2). For the diluted electrolyte a high amount of cumulated charge is detected directly after the start of the measurement. Compared to the more concentrated electrolytes it shows a steep slope and 26 C are generated after 72 h. This can on the one hand be explained by oxidative degradation of the electrolyte, as the electrolyte is not stable at 5 V *vs.* K|K$^+$, which is apparent in Figure 3a, even though the Al surface might have a different catalytic effect compared to the Pt surface. On the other hand, it is expected that severe Al dissolution occurs in this electrolyte. The high amount of cumulative charge for 3.0 M KFSI (21 C) can be correlated with a still relatively poor stabilization of the Al surface. In contrast, for the 4.0 M electrolyte, only 3 C of charge was detected, showing the positive impact of the high salt concentration on the stability of the Al surface.

Considering the discussion stated above, the increased electrochemical stability of the ACC in more concentrated electrolytes is clearly evidenced. The lack of "free" solvent

molecules in favor of CIPs and especially AGGs in HCEs suppresses anodic Al dissolution. Usually, Al^{3+}-ions would be generated at the Al surface due to the high potential and the low solution potential of Al metal which can instantly form complexes with FSI^-.[55] In that case, coordinating solvent molecules would form a solvation shell around the [Al-FSI] complexes, solve them into the electrolyte and free the Al surface for more degradation processes.[28,56,60] The lower the overall amount of solvent, the less "free" solvent molecules are present and fewer Al complexes will be dissolved. The lack of solvent molecules in HCEs therefore leads to a kinetic stabilization of the Al surface. However, compared to other CC measurements performed *e.g.* with LiTFSI and $LiPF_6$ based electrolytes, the results still show a high amount of side reactions in the high-voltage region.[37,55] This can also be seen

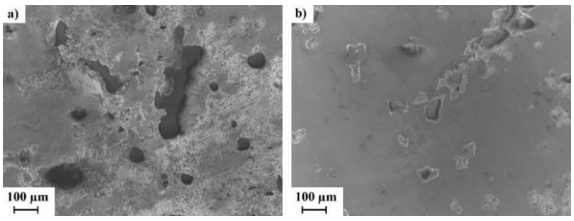

Figure 4. SEM images of the aluminium current collector after CC measurements, i.e., after potential hold at 5 V *vs.* $K|K^+$ for 72 h with a) 1.0 M and b) 4.0 M KFSI in EMC-based electrolytes.

in scanning electron microscopy images in Figure 4, that show severe pit formation even at high salt concentration.

Compared to prior measurements reported in literature (e.g. for LiTFSI/Pyr_{14}TFSI or LITFSI/ethyl methyl sulfone (EMS) electrolytes),[55,61] both the changed cation as well as the different anion that was used may be the driving force for the decreased electrochemical stability of the ACC. Especially FSI-based electrolytes are known to show severe Al dissolution compared to other imide-based electrolytes (such as TFSI or FTFSI), as previously reported by Beltrop et al.[45] In particular, electrolytes containing $TFSI^-$ (highly concentrated or in combination with ILs) or PF_6^- are more effective in stabilizing Al surfaces than FSI^- based ones and reveal the importance of the anion.[32,47] On the other hand, K^+ is a much weaker Lewis acid than Li^+. Therefore, interactions between solvent and cation are not as strong, as it is also indicated by the lower desolvation energy for potassium salts compared with their lithium counterparts.[62] Thus, the activation barrier for solvent molecules to leave the K^+ solvation shell and to take part in undesired side reactions is lowered. Considering this, the role of the cation on the Al dissolution should not be underestimated.

2.4. Electrochemical Performance Studies of K^+ and FSI^- Intercalation into Graphite in Graphite||K Metal Cells

In the following, the formation of donor- and acceptor-type graphite intercalation compounds (GICs) in KFSI-EMC-based electrolytes is comprehensively investigated, i.e., with respect to the K^+ intercalation into graphite negative electrodes and FSI^- intercalation into graphite positive electrodes.

By intercalation of anions at high potentials ($\geq$4.5 V *vs.* $K|K^+$), graphite is oxidized and $(FSI)C_x$ compounds with $x \gg 1$ are formed (acceptor-type GIC). In contrast, at low potentials ($\leq$ 4.5 V *vs.* $K|K^+$) reduction of graphite occurs and K^+ ions intercalate to form compounds with a maximum stoichiometry of KC_8 (donor-type GIC).[11,58] To simulate the behavior in graphite||graphite cells and to separate both electrode reactions, graphite||K metal cells are firstly investigated. In this cell setup, the graphite WE functions either as cation or anion host and is therefore investigated independently of each other *vs.* metallic K as CE.

The constant current charge/discharge cycling results (specific current: 100 mA g^{-1}) of graphite between cut-off potentials of 0.02 V and 1.5 V *vs.* $K|K^+$ in a graphite||K metal cell setup are depicted in Figure 5a and show only a minor dependence of discharge capacity (DC) and Coulombic efficiency (C_{Eff}) from salt concentration. A 1st cycle C_{Eff} of $\approx$76% is achieved for each of the electrolytes, independent of the salt concentration, although a more detailed look into the differential capacity plots (Figure S2) shows differences for between the "diluted" 1 M electrolyte and the HCEs (3.5 M and 4 M). During the 1st cycle, the highest onset potential can be seen for the 1 M electrolyte, suggesting that the SEI is built up at higher potentials, most likely due to oxidation of the carbonate solvents EC and EMC. These are much less concentrated in the HCEs, which therefore could show a different SEI formation behavior at lower potentials. A more detailed discussion on SEI formation and composition will follow in the next subchapter.

The DC nearly matches the theoretical capacity[11] of KC_8 with 279 mAh g^{-1} and an average C_{Eff} of more than 99.8% for the HCEs are achieved. Also, there is only a minor decrease in DC with cycling, after 200 cycles an impressive capacity retention of 99% is observed. Compared to potassium-based electrolytes already reported in literature, an improved rate capability as well as decreased capacity fade is visible (see Figure 1), as discussed above.[20,39,40,63] For the diluted 1 M KFSI/EMC electrolyte, same DCs are obtained with a slightly lowered and less sustained C_{Eff}.

In contrast, onset potentials for the cation (de-)intercalation differ (Figure 5b) for the more concentrated electrolytes. At 3.5 M and 4.0 M, both intercalation potentials at an arbitrary defined onset of -1.25 Ah g^{-1} V^{-1} are at 0.19 V *vs.* $K|K^+$, whereas K^+ intercalation in the diluted electrolyte is slightly shifted to lower potentials (0.14 V *vs.* $K|K^+$), suggesting that the charge transfer resistance decreases at higher salt concentration. There are two possible reasons for this behavior. On the one hand, an alteration of the SEI layer composition with improved kinetic properties could decrease the resistance.[26,29,64] On the other hand, different solution struc-

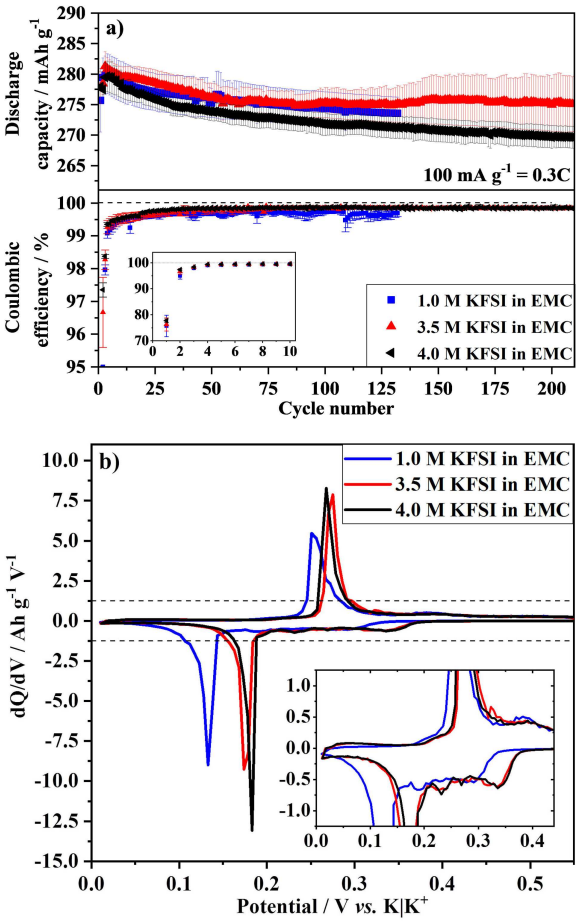

Figure 5. a) Specific DC and C_{Eff} for long-term charge/discharge cycling investigation of K^+ intercalation into graphite in graphite||K metal cells between the cut-off potentials of 0.01 V and 1.5 V *vs.* K|K^+ (half-cell setup) for 1.0 M, 3.5 M and 4.0 M KFSI in EMC electrolytes at a specific current of 100 mA g^{-1} (≈0.3 C; theo. cap.: 279 mAh g^{-1}). b) Differential capacity (dQ/dV) profiles of graphite||K metal cells showing the onset potentials of cation intercalation in the 10th cycle during charge/discharge at a specific current of 100 mA g^{-1}. Horizontal lines correspond to an arbitrary defined onset value of ±1.25 Ah g^{-1} V^{-1} for comparison of the onset potentials.

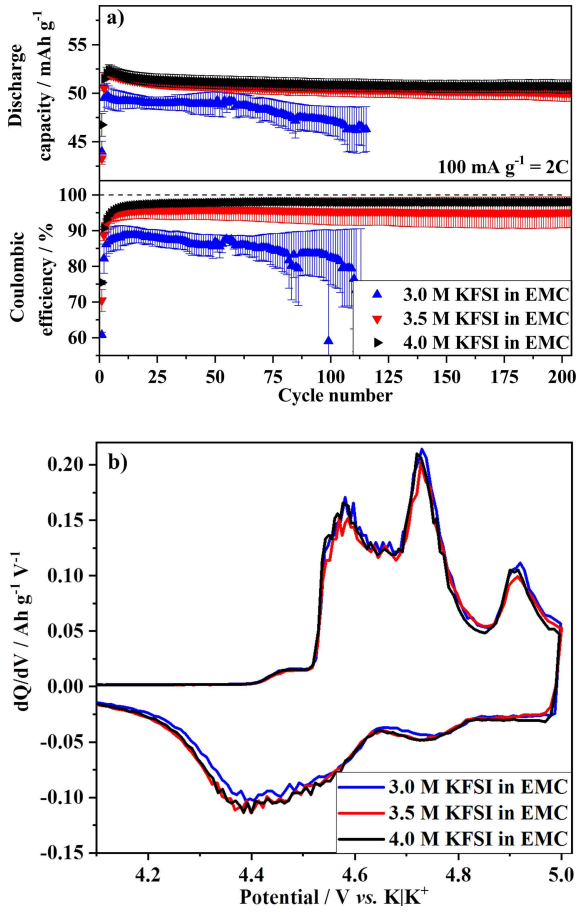

Figure 6. a) Specific DC and C_{Eff} for long-term charge/discharge cycling investigations of anion intercalation into graphite in graphite||K metal cells between the cut-off potentials of 3.4 V and 5.0 V *vs.* K|K^+ (half-cell setup) for 3.0 M, 3.5 M and 4.0 M KFSI in EMC electrolytes at a specific current of 100 mA g^{-1} (≈2C; theo. cap.: 50 mAh g^{-1}). b) Differential capacity (dQ/dV) profiles of graphite||K metal cells showing the onset potentials of anion intercalation in the 10th cycle during charge/discharge at a specific current of 100 mA g^{-1}.

tures at different salt concentrations could lead to an easier desolvation of the ions and therefore decrease the activation barrier of the whole intercalation process.[37] Especially the lack of solvent at higher concentrations in favor of ionic aggregates (AGGs, see above) diminishes the solvation shell and decreases the desolvation energy. Additionally, onset potentials for the de-intercalation of K^+ ions from the graphitic carbon host at the arbitrary defined onset of 1.25 Ah g^{-1} V^{-1} depend much less on the concentration of the electrolyte (0.25 V and 0.26 V *vs.* K|K^+, respectively). Combined, this results in a lowered voltage hysteresis for K^+ intercalation/de-intercalation processes into graphitic electrodes with HCEs, as the difference in (de-) intercalation potentials is decreased at high concentrations from ≈110 mV to ≈70 mV.

On the other hand, the electrochemical performance of the FSI^- intercalation into the positive electrode shows both an increasing DC and C_{Eff} with increasing salt concentration (Figure 6a).

The discharge capacity over cycling is very similar for the 3.5 M and 4.0 M electrolytes, even though the overall reversibility seems to depend strongly on the concentration. The reason seems not to be the intercalation/de-intercalation reaction itself, as there is no shift in the intercalation potentials (see Figure 6b), but rather additional parasitic reactions, especially for less concentrated electrolytes.

Changes in performance (DC and C_{Eff}) between the 3.5 M and 4.0 M electrolyte are small and almost within the standard deviation. As this is the case for both, anion and cation intercalation (*cf.* Figures 5 and 6), the following experiments are conducted with the 3.5 M HCE, as it shows the same performance compared with lower salt concentration and hence lowered viscosity and cost. On the contrary, the 3.0 M electrolyte shows a clearly worse performance for anion intercalation into the graphite positive electrode with respect to DC and C_{Eff}. The changes in DC and C_{Eff} for the anion intercalation are in agreement with the CC electrochemical measurements of the different electrolytes (*cf.* Figure 3b). The 3.0 M electrolyte does not passivate the ACC properly, as already shown above.

Anodic Al dissolution leads to a high amount of parasitic side reactions that minimize especially the C_{Eff} of the cells. As already explained above, Al^{3+} ions are formed at the Al surface at high potentials and will form complexes with the FSI anions, which are accumulated near the Al surface.[55] Usually, these Al-FSI complexes will be dissolved by EMC. The lack of solvent in favor of CIPs and AGGs inhibits dissolution of the aforementioned complexes and inhibits the ACC from severe Al dissolution.[28] In lower concentrated electrolytes, "free" solvent molecules are present and thus, the kinetic prevention of the dissolution of the Al/FSI containing surface coating is not sufficient. This is also one reason for the slightly lowered 1st cycle C_{Eff} for the FSI^- intercalation compared to the K^+ intercalation and the poor cycling performance at high potentials for the 3.0 M electrolyte. In previous studies, we reported that the first charge cycle of DIB cells is related to a "kinetic activation" (=first anion intercalation into graphite), which might result in a decreased C_{Eff}, compared to the following cycles.[16,19] This effect can be well observed by a shift of the onset potential for anion intercalation to lower values for the 2nd and following charge cycles, as previously discussed.[16,19]

To overcome the drawbacks related to the ACC, different strategies could be applied. Those include the use of protective coatings[61] or the exchange of the current collector to other materials such as TiN, which shows a much higher oxidative stability.[65,66] *Kravchyk* et al. reported on a DIB cell based on FSI^- intercalation into a graphitic cathode. Using TiN instead of Al as current collector for the positive electrode, higher potentials and thus higher DCs were reached with a sufficient stability. On the other hand, Al is the material of choice due to a variety of reasons, as explained above.

In Figure 7, the influence of different specific currents on the intercalation behavior of K^+ (Figure 7a) and FSI^- ions (Figure 7b) into graphite is shown.

Anion intercalation studies of the 1.0 M KSFI electrolyte in the potential range from 3.4 V to 5.0 V *vs.* $K|K^+$ could not be executed, as severe oxidative degradation of the electrolyte and ACC dissolution occurred.

The obtained DC for the FSI^- intercalation shows only a minor dependence of the applied C-rate, it differs between 45 mAh g^{-1} and 50 mAh g^{-1} for the different rates, while it shows the lowest capacity for the lowest charge/discharge rate (Figure 7b). The effect of the specific current on the C_{Eff} is much stronger than for the DC. For the lowest rate of 0.1 C the C_{Eff} is only ≈78.0% and raises up to 99.7% for 5 C. An explanation can be given with the total time spent at positive electrode high potential. The higher the current rate, the faster the charging and discharging happens and therefore the time in the critical potential region of more than 4.5 V *vs.* $K|K^+$ is lowered, *i.e.*, parasitic side reactions including anodic Al dissolution and electrolyte decomposition will be reduced. In summary, a high charge/discharge rate leads to an enhanced C_{Eff}.

The potassiation of graphite in a potential range of 1.50 V to 0.01 V *vs.* $K|K^+$ displays a high C_{Eff} exceeding 99.8% for each specific current, except for the first cycles which are mainly

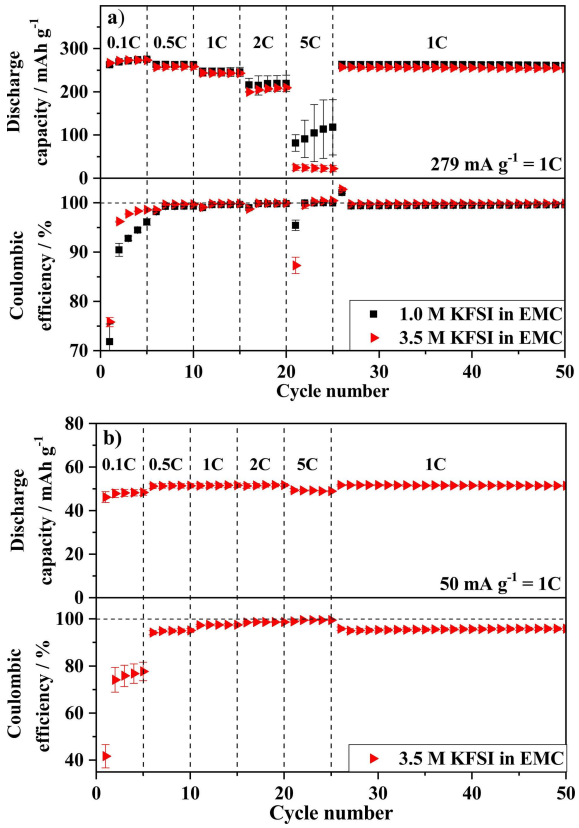

Figure 7. a) Specific DC and C_{Eff} for K^+ intercalation into a graphite negative electrode (0.01 V and 1.50 V *vs.* $K|K^+$) and b) specific DC and C_{Eff} for FSI^- anion intercalation into a graphite positive electrode (3.4 V and 5.0 V *vs.* $K|K^+$) for 1.0 M and 3.5 M KFSI in EMC electrolyte for graphite||K metal cells (half-cell setup) at various specific currents.

influenced by the SEI formation (Figure 7a). The DC shows a pronounced decrease for C-rates greater than 2 C, with values exhibiting ≈200 mAh g^{-1} at 2 C and ≈60 mAh g^{-1} at 5 C. Especially at lower current, only a small difference is obtained for the 1.0 M and the 3.5 M electrolyte. A higher DC at higher specific current for the diluted electrolyte on the other hand can be assigned to the physical characteristics of the electrolyte. The diluted electrolytes have a much lower viscosity than their highly concentrated analogues and consequently a higher ionic conductivity.[22,25] Both are essential for a good performance at high rates due to higher ionic mobility.

However, the differences are very small, which is in contrast to previous results reported for lithium-based cells. Graphite||Li metal cells with diluted $LiPF_6$ issolved either in DMC or EMC as electrolyte showed a lower C_{Eff} as well as a reduced DC compared to their highly concentrated analogues.[27] This is strongly related to different SEI formation processes at the graphite negative electrode in these electrolytes. In diluted, i.e. 1 M electrolytes, the overall cell performance and structure of the SEI layer for cells cycled with $LiPF_6$, LiTFSI or LiFSI-containing electrolytes is comparable, if EC is used as co-solvent.[67] This is due to preferential degradation of the EC solvent, leading to a carbonate-derived SEI. On the other hand it was found, that SEI layers derived from HCEs have a different

structure and consist of an increased amount of lithium and fluorine.[26] Because of the lack of "free" solvent in favor of ion aggregates, the passivating SEI film is rather dominated by decomposition products of the anions instead of solvent molecules, as in diluted electrolytes.

EC is known to form an effective SEI via electrochemical reduction at potentials of ≈0.8 V *vs.* Li/Li^+.[35,41] From a theoretical point of view, the lowest "lowest unoccupied molecular orbital (LUMO)" of the molecules takes part in the reaction and will be reduced first.[26,29,31] The electrolyte used in this work does not contain EC and thus, only the LUMOs of EMC and FSI^- are left to take up an electron during reduction. As FSI-based salts are also used as additive to form a more effective and better conducting SEI layer in LIBs, they are likely to be reduced earlier even in diluted electrolytes.[68–72]

2.5. Characterization of the Solid Electrolyte Interphase Composition

Highly concentrated lithium-based electrolytes are known to form a SEI consisting mainly out of degraded anions. These build up an effective interphase and reduce active lithium losses in the following cycles compared to diluted electrolytes.[26,29,31,33,34,73,74] There are two main explanations for this behavior. On the one hand, a negligible amount of non-coordinating or co-intercalating solvent molecules is present and can be degraded to form a passivating SEI film.[26,29] Next to this kinetic effect, a change in electronic states, especially of the anion, plays a major role in explaining the stabilization thermodynamically. Due to the formation of CIPs and AGGs, much stronger ion-ion interactions occur in HCEs. This leads to a change in the orbital states of the anion. *Sodeyama* et al. showed, that for LiTFSI the LUMO of the $TFSI^-$ anion is lowered due to partial donation of an excess electron to interacting Li^+ ions in the AGG state.[29] By surpassing the solvents' LUMO, the LUMO of the anion becomes the LUMO of the overall electrolyte. Transferred to the KFSI/EMC electrolyte, reduction of the anion would be thermodynamically preferred to EMC reduction in HCEs. Enhanced FSI anion degradation takes place, which should correlate with a higher amount of reduction components from the anion, especially fluorides, in the SEI layer. Furthermore, it has to be noted that K^+ ions are much weaker Lewis acids than Li^+ ions, so it is questionable whether the mechanism, which is evidenced in LIBs, takes place in potassium-based cells and electrolytes as well. On the other hand, FSI^- is known to be electrochemically less stable than $TFSI^-$, as it is also used as electrolyte additive for building up an effective SEI.[67–69,71,72] Considering this, a tendency to build up an effective SEI with comparable high amount of anion degradation products is given, maybe even for diluted electrolytes with merely 1.0 M salt concentration. This is also supported from the differential capacity measurements presented in Figure S2 (Supporting Information). They show a relative similar onset potential for the reduction reaction at ≈0.35-0.40 V *vs.* $K|K^+$ for the diluted 1 M electrolyte and the HCEs, while the onset potential for reductive decomposition of the HCEs is slightly shifted to lower potentials. This hints a decomposition of carbonate solvents at higher potentials compared to the HCEs, where the solvent is much less concentrated. Therefore, a different SEI layer with different properties may be formed. However, no systematic study of SEI layers derived from potassium-based electrolytes has been performed yet. To further investigate and support the formerly given considerations, XPS measurements have been performed to compare details of the formed SEI layers in different electrolytes.

XPS is used to show the exact composition of the SEI. In Figure 8, the XPS spectra of graphite negative electrodes are shown, obtained from graphite||K metal cells after 5 charge/discharge cycles in 1.0 M, 3.5 M and 4.0 M KFSI in EMC electrolytes. Additionally, the total amount of the respective atoms in the measured surface layer is given in Table 3. With increased salt concentration the amount of "inorganic" fluoride (KF) decreases, while the "organic" fluoride species (fluorosulfoxide species) slightly increase. The amount of O and K atoms in the SEI surface layer decreases as well, whereas N, S and C increase. Therefore, the increased amount of N, S and "organic" F suggests an increase of FSI anion degradation products in HCEs.[29,73]

Table 3. Total amount of atoms in the SEI surface layer at a graphite negative electrode. Prior to measurement, 1.0 M, 3.5 M and 4.0 M KFSI in EMC electrolytes were cycled at a specific current of 28 mA g^{-1} for 5 charge/discharge cycles in a graphite||K metal cell setup. Values are obtained from results also shown in Figure 8.

Element	1 mol L^{-1} [at%]	4 mol L^{-1} [at%]
Fluorine ("organic")	4.20 ± 0.23	4.72 ± 0.24
Fluorine ("inorganic")	3.64 ± 0.24	1.36 ± 0.09
Nitrogen	4.28 ± 0.24	6.60 ± 0.89
Sulfur	7.62 ± 0.10	8.82 ± 0.76
Oxygen	25.18 ± 0.48	21.62 ± 1.25
Potassium	14.30 ± 0.15	11.76 ± 0.82
Carbon	40.78 ± 1.22	45.12 ± 3.94

Another hint is given by a more detailed look on the relative occurrence of N, S and F. In the FSI anion, they show a ratio of N:S:F = 1:2:2, which is consistent with the results obtained from the 1.0 M electrolyte. After increasing the concentration, however, the ratio shifts towards N:S:F ≈1:1:1.5. This change shows, that there is not only a higher amount of SEI components originating from the anion, but that the FSI anion is decomposed more strongly at a higher salt concentration in the electrolyte as well.

It has to be noted that the differences between the concentrated electrolytes are small, so a more detailed study is needed to prove this finding. Measurements in lithium-based electrolytes showed much stronger differences between the solvent-derived SEI in diluted and anion-derived SEI in HCEs. The reason seems to be the FSI^- anion as well as the changed cation. It is already known, that FSI^- as conducting salt in diluted electrolytes increases the amount of inorganic fluoride (LiF) in the SEI.[75] Therefore, it has similar properties with respect to reductive anion decomposition as is reported for

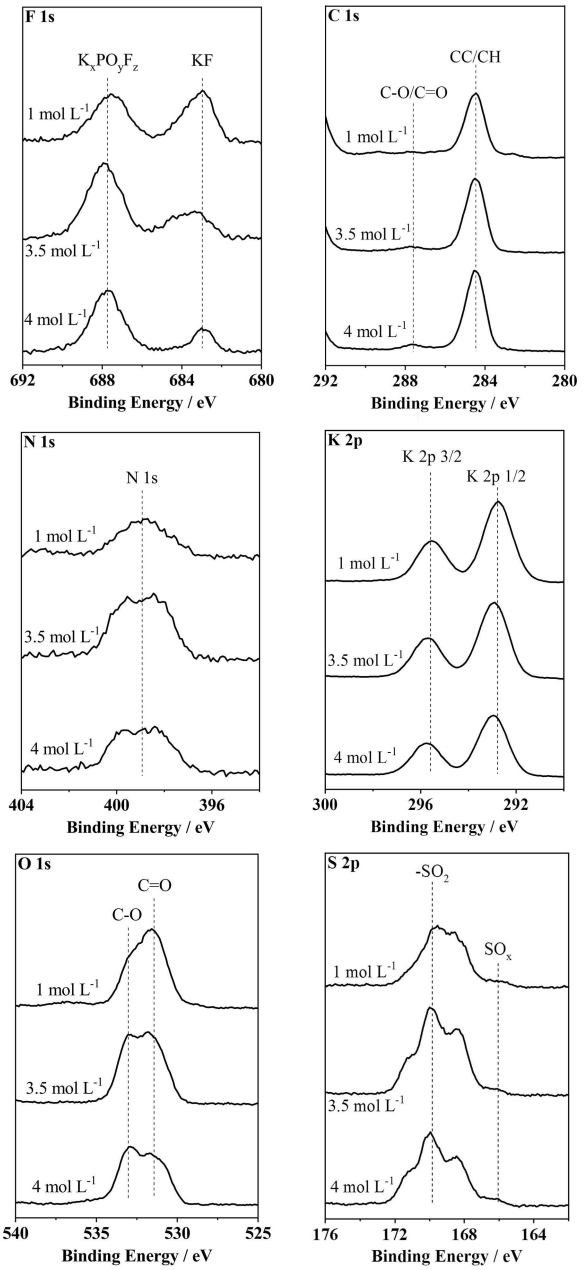

Figure 8. XPS spectra of graphite negative electrodes cycled for 5 charge/discharge cycles at a specific current of 28 mA g^{-1} in 1.0 M, 3.5 M and 4.0 M KFSI in EMC electrolyte in a graphite||K metal cell setup (half-cell setup; 1.50 V to 0.01 V *vs.* K|K$^+$). The graphite WE was washed with EMC and measured without exposure to air.

highly concentrated-based electrolytes. Therefore, increasing the salt concentration of an FSI-based electrolyte leads only to a minor increase in inorganic fluorides compared to increased concentrations for electrolytes with a different conducting salt. Simultaneously, the relatively weak Lewis acidity of K^+ compared to Li^+ leads to a high amount of K^+ ions in the SEI.

In summary, highly concentrated KFSI-based electrolytes show preferred anion degradation at low potentials for K^+ intercalation into graphite rather than degradation of the solvent. In principle this should lead, similar to lithium-based HCEs, to an interphase with enhanced kinetic properties for K^+ ions. However, the difference in the SEI composition as determined by XPS is very small, and therefore only small differences in the kinetic properties occur, which can be seen in a slightly lowered hysteresis at higher concentrations (70 mV to 110 mV, *cf.* Figure 5). Additionally, similar processes seem to occur at low salt concentrations due to low Lewis acidity of K^+, higher reductive stability of EMC than EC as (co-)solvent and lower reductive stability of FSI^- compared to other conducting salts. This would potentially offer a variety of possibilities of PIBs with altered and maybe reduced charge-transfer resistances for the SEI.

2.6. Electrochemical Performance of a Potassium-Based Dual-Graphite Battery Cell

Graphite shows very promising properties as negative as well as positive electrode material, as previously discussed for graphite||K metal cells for cation and anion intercalation with the here introduced electrolyte systems. Combining both approaches results in a dual-graphite battery (DGB) cell applying 3.5 M KFSI in EMC as electrolyte and graphite as negative and positive electrode material with a balancing of 1:1 based on the masses of the electrodes. This DGB system serves as model system for better understanding of the performance of DGB cells, thus the capacity balancing is not yet optimized. The 3.5 M KFSI HCE was chosen over the more concentrated 4.0 M counterpart due to similar performances in graphite||K metal cells with simultaneously lower salt content. The slightly lowered concentration improves physical properties like viscosity and ionic conductivity.

The results for long-term cycling as well as C-rate performances (see Figure 9) are very similar to those obtained in the graphite/potassium metal cell systems (*cf.* Figures 5–7). On the one hand, with increasing specific current, the DC decreases from 50 mAh g^{-1} at 5 mA g^{-1} down to 20 mAh g^{-1} at 250 mA g^{-1}. The CE on the other hand increases with increasing specific current up to a maximum of >99.0%. This was also observed for the anion intercalation into graphite in a graphite||K metal cell. Therefore, similar explanations hold for the DGB cell, i.e., parasitic side reactions like anodic Al dissolution or oxidative electrolyte degradation cannot be fully avoided at high cell voltages, i.e. graphite electrode potentials. A higher current corresponds with less time spent at critical potentials and the parasitic reactions are scaled down to a minimum. However, especially the rate capability is not as good as in K-DGB cells with ILs as electrolyte solvents.[19] It can be assumed that the high viscosity of the electrolyte and, consequently, the reduced ionic conductivity are an explanation.

Furthermore, a very reversible long-term cycling can be seen. In Figure 9b, the long-term charge/discharge cycling behavior at a specific current of 50 mA g^{-1} is depicted and shows a capacity retention of 76% after 200 cycles (based on the 1st cycle after formation) with an average C_{Eff} between 90–95%.

This is, once more, a result of the relatively high anodic Al dissolution of the ACC. In particular, it also needs to be

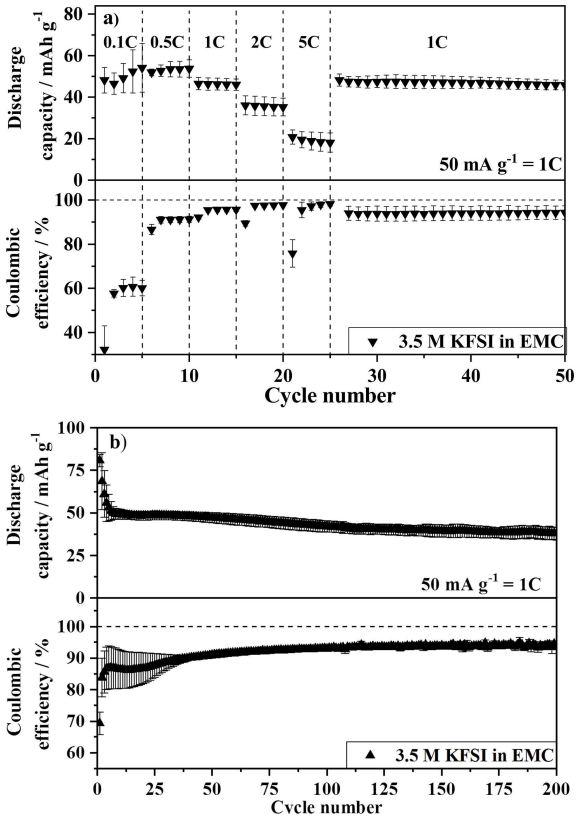

Figure 9. Specific DC and C_{Eff} a) at various specific currents and b) for long-term charge/discharge cycling at 50 mA g^{-1} (=1) in graphite||graphite cells (full cell setup; voltage range: 3.4 V–5.0 V) with a 3.5 M KFSI in EMC electrolyte. Prior to measurement, formation was conducted for 5 cycles at 5 mA g^{-1} (0.1 C).

considered that the salt concentration will be reduced during each charge step as cations and anions are removed from the electrolyte, *i.e.*, an enhanced Al dissolution at the positive electrode will take place at the highest state-of-charge. However, if protective coatings or other current collector materials such as TiN were applied the cycling performance may be further improved.[61,65] Next to this, an initial "activation process" for the C_{Eff} is noteworthy, i.e., the C_{Eff} increases from ≈85% to ≈95% over cycling (Figure 9b). This increase is most likely due to several reasons: The dissolution of the Al current collector and the decomposition of anions at or within the graphite host structure will result in the formation and growth of decomposition/surface layers at the positive electrode (i.e., cathode electrolyte interphase, CEI), which will most likely reduce parasitic reactions and, thus result in an increase of C_{Eff} over cycling. Furthermore, due to parasitic reactions and a shift of the electrode potentials during cycling, K metal is irreversibly plated on top of the negative electrode (see further explanations below). This effect is intensified upon cycling and leads to a decrease of the positive electrode potential, which ultimately reduces parasitic reactions related to the dissolution of the Al current collector (see also Figure S3, Supporting Information). However, we observed a relatively high standard deviation of the C_{Eff}, especially in the first charge/discharge cycles, preventing a more detailed look on the respective mechanisms and hinting on different "activation processes".

For DGB cells, a suitable capacity balancing between the negative and positive electrode (N/P ratio) needs to be ensured to avoid metal plating at the negative electrode, similar to lithium ion cells.[76] Recently, we reported on the origin of capacity fading and aging mechanisms in DGB cells, which are induced by parasitic reactions at either the positive or negative graphite electrode.[53] Parasitic currents, that are for example apparent at the positive electrode (=generation of electrons), due to Al dissolution at high potentials and/or (electro-) chemical oxidation of the electrolyte, will lead to an ongoing irreversible accumulation of K^+ ions in the negative graphite electrode, as a result of charge neutrality. These irreversibly stored K^+ ions will therefore reduce the reversible storage capacity of the negative electrode. We explained this capacity fading mechanism with an electron inventory model which is valid for DGB cells.[53] As the dissolution of the ACC and/or (electro-)chemical oxidation of the electrolyte is an ongoing process, which can be observed by the rather low C_{Eff} of only 90–95%, the negative electrode is filled with more and more K^+ in each cycle. At a certain point, the electrode is completely filled and potassium will be reversibly plated and stripped at the top of the graphite negative electrode. Heidrich et al. reported a similar phenomenon for lithium-based DGB cells, in which vinylene carbonate (VC) was added to an electrolyte consisting of 3.5 M $LiPF_6$ in EMC. Due to the oxidative decomposition of VC at the positive electrode, Li^+ ions were irreversibly intercalated into the graphite negative electrode to keep charge neutrality of the DGB cell. In turn, Li metal was reversibly plated/stripped at the negative electrode during charge/discharge operation of the DGB cell.[53]

In case of the K-DGB cell, this degradation process is apparent especially for long-term cycling at low specific currents, as the irreversible parasitic reactions depend on the time spent at high potentials and not on the cycle number itself. This degradation is exemplarily shown in Figure 10a. Due to low specific current in the beginning of the experiment, the time spent at critical potentials is increased and leads to increased dissolution of the ACC and/or (electro-)chemical oxidation of the electrolyte and finally to plating/stripping of K metal on the negative electrode during charge. The ongoing accumulation of cations at the anode can be observed by a decrease of the anode potential, which drops below 0 V *vs.* $K|K^+$ after ≈200 cycles (≈500 h; see red arrow). It has to be mentioned that this cation accumulation should not be mixed up with the decreasing anode potential during the rate investigation, as the anode potential drops below 0 V *vs.* $K|K^+$ at the highest rate of 5 C (=250 mA g^{-1}), *i.e.* at ≈300 h (Figure 10a). This drop is most likely related to high over-potentials for K^+ intercalation at the negative graphite electrode. However, when the charge/discharge rate is reduced, the anode potential rises again above 0 V *vs.* $K|K^+$. As the DGB cell is cycled via control of the cell-voltage, a decrease of the anode potential is accompanied by a decrease of the cathode potential. In the given case, the potential at the cathode drops from 5.1 V *vs.* $K|K^+$ in the first cycles to only 4.95 V *vs.* $K|K^+$ for

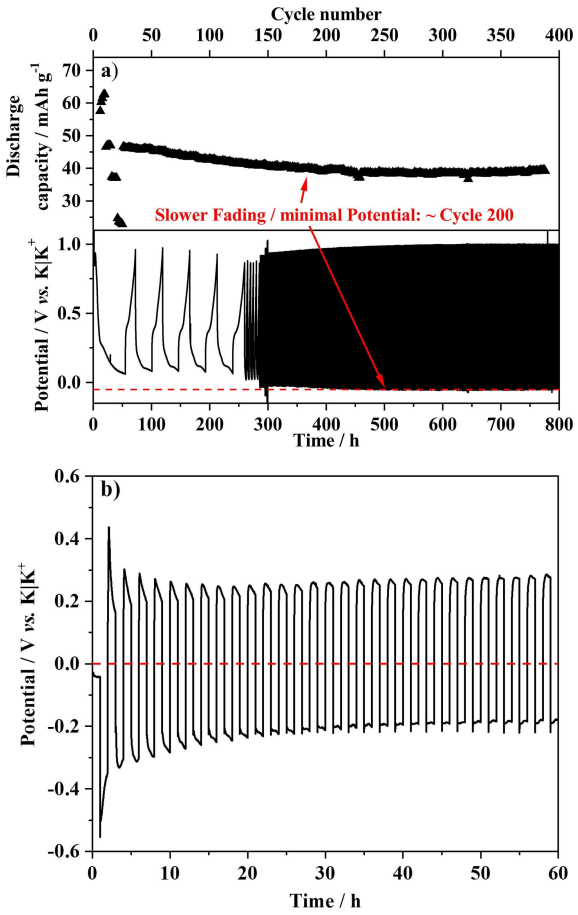

Figure 10. a) Specific DC and graphite negative electrode potential of a graphite||graphite cell (full-cell setup) with 3.5 M KFSI in EMC electrolyte, cycled in a voltage range of 3.4 V and 5.0 V at a specific current of 50 mA g^{-1} after investigating different specific currents in the first 25 cycles. b) Reversible plating and stripping of K metal in symmetrical K metal||K metal cells at a current of 0.15 mA, which is comparable to the 50 mA g^{-1} for the DGB cell in (a).

each cycle after the 200th cycle. In turn, this corresponds to a minimum negative electrode potential of ≈ -0.05 V *vs.* K|K^+ (marked as red line in Figure 10a, and in Figure S3). The DC strongly depends on the cathode potential (*cf.* Figure 6b) and even a small potential decrease results in a huge loss of reversible capacity.

Therefore, a decreased negative electrode potential correlates with a decreased DC as shown in Figures 10 and S3 (Supporting Information). At first, a fading of DC and a decrease in negative electrode potential occur simultaneously due to continuous K^+ ion accumulation in the negative electrode (Figure S3). Once the negative electrode is completely and irreversibly filled with intercalated K^+, plating/stripping of additional K metal starts and a "hybrid graphite||K metal cell" is created.

The reversible stripping and plating process of K metal in symmetrical K metal||K metal cells is depicted in Figure 10b. The process occurs at a defined potential and is highly reversible, therefore no more decrease in anode potential and ultimately no more fading of DC is visible and a stable cycling can be seen in the "hybrid graphite||K metal cell". This concept is complementary to reversible cycling of graphite||Li metal DIB cells, although in those cases *e.g.* artificial coatings or other measures are needed to stabilize the highly reactive metallic Li negative electrode in order to guarantee a sufficient long-term cycling stability without safety issues.[77] Nevertheless, it has to be kept in mind that the K metal plating and stripping also results in overpotential of $\geq$200 mV, which has a direct impact on the positive electrode potential, which will be further decreased within the charge step. Further, it has to be mentioned that we chose a highly capacity-overbalanced negative electrode (mass ratio of N to P = 1:1, which equals a N/P ratio of >5; based on practical capacities at 1 C: N$\geq$ 250 mAh g^{-1} and P$\approx$50 mAh g^{-1}). In turn, in an energy-optimized cell, *e.g.* using an N/P ratio of 1.1 to 1.2, K metal plating would occur in even earlier cycles. Therefore, future studies on electrolyte optimization and stabilization of the interphases (SEI, CEI) are mandatory to reduce parasitic side reactions.

Another major drawback of DIB and DGB cells is a relatively high self-discharge reaction when stored in a charged state, *e.g.* at $\approx$5 V.[16] Figure S4 shows that this behavior is also apparent in the here presented K-DGB cells. After 10 h at an open-circuit voltage state, the cell voltage dropped from 5.0 V to $\approx$4.3 V, which is even worse compared to measurements in Li metal-based DIB cells.[16] The reasons for this different behavior are most likely the different cell setup and electrolyte (*e.g.*, K^+ intercalation/de-intercalation into graphite *vs.* Li metal plating/stripping, ionic liquid electrolyte *vs.* organic solvent-based electrolyte), so that interface reactions at both the negative and positive electrode are completely different and cannot be compared to each other. Additionally, Al dissolution is a severe challenge at the high positive electrode potentials and may lead to enhanced self-discharge as well. Further comprehensive studies are mandatory to elaborate the self-discharge mechanism in DGB cells in dependence of the electrolyte. Overall, the reduction of self-discharge, next to an improved capacity retention and avoidance of metal plating are needed to further optimize K-DGB cells.

In summary, capacity fading mechanisms need to be considered and further evaluated when studying novel dual-graphite battery cells. The investigation in two-electrode cells, such as coin cells, may lead to misinterpretations of the cycling performance, especially when metal plating/stripping at the negative electrode occurs. Therefore, we strongly recommend to elaborate the storage mechanism of DGB cells also with respect to changes of the individual electrode potentials, *e.g.* in a suitable cell setup with a reference electrode.

3. Conclusion

In this work, an alternative, potentially low-cost potassium-based dual-graphite battery (K-DGB) in combination with highly concentrated electrolytes (HCEs) is presented. HCEs based on the conducting salt potassium bis(fluorosulfonyl)imide (KFSI) and ethyl methyl carbonate (EMC) as single solvent form an

electrolyte with desired properties for dual-graphite (electro) chemistry. With Raman spectroscopic measurements, aggregation of ions at high concentrations is shown. This, in combination with a lack of free solvent molecules, leads to an increased oxidative stability of the electrolyte exceeding 5 V *vs.* $K|K^+$. For the same reason, anodic dissolution of the Al current collector (ACC) at the positive electrode is remarkably decreased.

Investigations in graphite||K metal cells show the reversible charge and discharge cycling. Especially a high discharge capacity (DC) near the theoretical capacity of 279 mAh g^{-1} for K^+ ion intercalation into the graphite negative electrode is noteworthy and exceeds the performance of potassium-based electrolytes currently known in literature. Differences in cycling behavior between diluted and HCE are small, however, result in a decreased voltage hysteresis at higher concentrations. Using graphite as host material for FSI anion intercalation, a DC of 50 mA g^{-1} was obtained with a capacity retention of 76% after 200 cycles (based on the 1st cycle after formation).

By means of X-ray photoelectron spectroscopy, differences in solid electrolyte interphase (SEI) formation are investigated for the diluted and the HCE. It was shown, that the SEI contains more degradation products of the FSI salt at high concentrations. This principally should decrease charge transfer resistances and can be seen as cause for the decreased voltage hysteresis using HCEs.

Following the invention of the electrolyte and its validation in graphite||K metal cells, graphite||graphite (DGB) cells were investigated and the capacity fading mechanism was elaborated. Due to the characteristic simultaneous (de-)intercalation of cations and anions into their respective electrodes during charge and discharge, parasitic reactions such as the dissolution of the ACC and/or oxidative decomposition of electrolyte ingredients leads to accumulation of K^+ ions in the negative electrode. Ongoing filling and ultimately plating of K metal onto the negative electrode goes hand in hand with the decrease in the negative electrode potential. Hence, cycling via control of the cell-voltage causes a simultaneous decrease of potential on the positive electrode side and thus decreases the capacity gained by anion intercalation.

In summary, high salt concentrations of KFSI in EMC as electrolyte enable highly reversible cycling in potassium-based DGB cells. By increasing the anodic stability of the ACC, a low-cost and "green" battery system was proposed. However, challenges with respect to capacity fading and metal plating at the negative electrode have not been resolved yet, and need further comprehensive analysis.

Experimental Section

Electrode and Electrolyte Preparation

Graphite electrodes were used for the positive and negative electrode (in case of a DGB cell setup) and contained 90 wt.% of the active material (KS6 L graphite, Imerys Graphite & Carbon), 5 wt.% carboxymethylcellulose (Walocel CRT 2000 PPA 12, Dow Wolff Cellulosics) as binder and 5 wt.% conductive agent (carbon black C-nergy SuperC65, Imerys Graphite & Carbon) casted on an aluminium foil (Evonik Industries; purity ≥ 99.9%). The punched electrodes had a diameter of 12 mm and an average active material mass loading of 2.0 ± 0.1 mg cm^{-2}. Balancing of negative and positive electrodes (N/P ratio) was 1:1 based on the active masses. Therefore, the high overbalancing of the negative electrode allows for a more detailed look on SEI formation processes with limited amount of cross-talk from the positive electrode, as will be discussed below. The preparation process of the electrodes was performed as reported in our previous publication.[18]

For the preparation of the different electrolytes, the following reagents and materials were used: Ethyl methyl carbonate (EMC; BASF; purity: ≥ 99.0%) and potassium bis(fluorosulfonylimide) (KFSI; Solvionic; purity: ≥ 99.9%) were purchased and used as received. Electrolytes were prepared by dissolving KFSI in EMC in steps of ≈0.5 mol L^{-1} to the highest possible molarity (4.0 M). KFSI was chosen as conducting salt due to solubility challenges with other potassium salts, especially with KPF_6.[9] The electrolyte preparation and storage as well as the cell manufacturing were carried out in an argon filled glove box (H_2O and $O_2 < 0.1$ ppm).

Cell Preparation and Electrochemical Characterization

The electrochemical measurements were performed in Swagelok type T-cells in a three-electrode configuration (half-cell setup and full-cell setup[78]) as described previously.[15,18] In a graphite|| potassium (K) metal DIB cell setup (half-cell setup), the reference electrode (RE) as well as the counter electrode (CE) each consisted of metallic potassium (Sigma-Aldrich; purity: ≥ 99.9%), while the working electrode (WE) was graphite (either studied for K^+ or for FSI^- intercalation). For investigations of DGB cells, graphite was used as both the negative and positive electrode. In each cell, a glass microfiber filter separator (Whatman, grade GF/D) with 8 mm (RE) and 13 mm (between negative and positive electrode) diameter was utilized as separator and soaked with 80 μL or 120 μL electrolyte, respectively.

All constant current charge/discharge cycling experiments were performed on a Maccor 4000 battery test system. Graphite||K metal cells (half-cell setup)[78] with graphite as WE were studied with respect to anion intercalation with a constant current of 1 C = 50 mA g^{-1} (determined from the active mass and the practically achieved discharge capacity of the graphite positive electrode) in a potential range of 3.4 V and 5.0 V *vs.* $K|K^+$. On the other hand, for investigations of K^+ intercalation into graphite in graphite||K metal cells (half-cell setup), a specific current of 279 mA g^{-1} (corresponding to a rate of 1 C; determined from the active mass and the practically achieved discharge capacity of the graphite negative electrode) between the cut-off potentials of 0.02 V and 1.5 V *vs.* $K|K^+$ was applied. In DGB cells, measurements were performed at a specific charge/discharge current of 50 mA g^{-1} in a cell voltage range of 3.4 V and 5.0 V (full-cell setup). This setup allows to monitor the individual potentials (*vs.* $K|K^+$) of graphite negative and positive electrodes.[78] To investigate the electrochemical behavior at different specific currents, each 5 charge/discharge cycles at 28 mA g^{-1}, 140 mA g^{-1}, 279 mA g^{-1}, 558 mA g^{-1} and 1395 mA g^{-1} (0.1 C, 0.5 C, 1 C, 2 C and 5 C for K^+ intercalation into graphite) or 5 mA g^{-1}, 25 mA g^{-1}, 50 mA g^{-1}, 100 mA g^{-1} and 250 mA g^{-1} (for FSI^- intercalation into graphite), respectively, were applied, before further cycling was performed at 1 C. A C-rate of 1 was based on a specific current of 279 mA g^{-1} (= theoretical capacity of 279 mAh g^{-1} for K^+ intercalation) and a specific current of 50 mA g^{-1} (= 50 mAh g^{-1} for FSI^- intercalation into graphite), respectively. Chronocoulometry (CC) measurements have been performed to study the stability of the aluminium (Al) current collector. Therefore, Al foil was used as WE and K metal as CE and

RE (half-cell setup). The Al WE (surface area: 1.13 cm^2) was polarized linearly using a VMP3 potentiostat (Bio-Logic Science Instruments) within 1 h from open circuit potential up to 5.0 V *vs.* $K|K^+$ and hold at this potential for 72 h to measure the charge. Linear sweep voltammetry (LSV) measurements to investigate the electrochemical stability window (ESW) of the electrolytes were conducted using a VSP instrument (Bio-Logic Science Instruments) with a platinum electrode as WE and K metal as CE and RE (half-cell setup). The surface area of the platinum was $7.85 \cdot 10^{-3}$ cm^2 and a scan rate of 1 $mV s^{-1}$ from open circuit potential to a cut-off potential of 7 V *vs.* $K|K^+$ was applied.

The error range for the measured data was calculated by the standard deviation of three cells and the exact value is mentioned in the captions of the figures and tables. The axis labels do not display the correct significant digits for the clarity of the figures.

Characterization of the Al Current Collector Surface

The examination of the surface morphology of the Al WE, taken from the CC measurements, was made by scanning electron microscopy (SEM). The SEM images were taken by a Carl Zeiss AURIGA SEM microscope (Carl Zeiss Microscopy GmbH) with an acceleration voltage of 3 kV.

Characterization of the Ion Environment in Highly Concentrated Electrolytes

A FT-Raman/IR RAM II spectrometer by Bruker was used to study the electrolytes with different salt concentrations. The electrolytes were measured under an argon atmosphere to avoid degradation due to contact with oxygen or water. 1000 scans in the region between $\tilde{\nu} = 0$ cm^{-1} and $\tilde{\nu} = 4000$ cm^{-1} were performed. The spectra were normalized regarding to the band created by ν_{SNS} stretching modes of the bis(fluorosulfonyl)imide (FSI) anion at 740 cm^{-1} to the respective concentrations.[49] The analysis and deconvolution of the generated data was performed using the software "OPUS" (Bruker). The measured bands could be fitted numerically by superposition of corresponding, underlying bands. In this work, Lorentz-functions were generated and optimized with the Levenberg-Marquardt algorithm.

X-Ray Photoelectron Spectroscopy

X-ray photoelectron spectroscopy (XPS) was performed to analyze the initial SEI formation at the negative graphite electrode with different concentrated electrolytes. Graphite||K metal cells were cycled 5 times with a specific current of 5 $mA g^{-1}$ in a potential range of 0.02 V and 1.5 V *vs.* $K|K^+$. After disassembling in an argon filled glovebox (O_2 and H_2O both below 0.1 ppm), the electrodes were washed via dipping in 1 mL of EMC to remove electrolyte and salt residues. Afterwards, the electrodes were transported to the XPS device (Axis Ultra DLD, Kratos) without exposure to air. A monochromatic Al K_α source ($h\nu = 1486.6$ eV) with a 10 mA emission current and 12 kV accelerating voltage source power was used. The measurement was carried out at a 0° angle of emission and a pass energy of 20 eV. To compensate charging of the sample, a charge neutralizer was used. The fitting of the obtained spectra was performed with CasaXPS and calibration of the binding energy with the C 1s C–H/C–C peak at 284.5 eV as internal reference. Three different measurement spots per sample were investigated to guarantee a high reproducibility.

Acknowledgements

The authors wish to thank the Federal Ministry of Education and Research (BMBF) for funding this work in the project "Dual-Carb" (03XP0118).

Conflict of Interest

The authors declare no conflict of interest.

Keywords: anion intercalation · dual-graphite battery · electrolytes · graphite · potassium-based dual-ion battery

[1] a) M. Winter, *Z. Phys. Chem.* **2009**, *223*, 1395–1406; b) B. Dunn, H. Kamath, J.-M. Tarascon, *Science* **2011**, *334*, 928–935; c) O. Gröger, H. A. Gasteiger, J.-P. Suchsland, *J. Electrochem. Soc.* **2015**, *162*, A2605–A2622.
[2] a) M. Winter, B. Barnett, K. Xu, *Chem. Rev.* **2018**, *118*, 11433–11456; b) R. Wagner, N. Preschitschek, S. Passerini, J. Leker, M. Winter, *J. Appl. Electrochem.* **2013**, *43*, 481–496.
[3] J. Betz, G. Bieker, P. Meister, T. Placke, M. Winter, R. Schmuch, *Adv. Energy Mater.* **2018**, *334*, 1803170–1803187.
[4] a) T. Placke, R. Kloepsch, S. Dühnen, M. Winter, *J. Solid State Electrochem.* **2017**, *21*, 1939–1964; b) G. E. Blomgren, *J. Electrochem. Soc.* **2017**, *164*, A5019–A5025; c) R. Schmuch, R. Wagner, G. Hörpel, T. Placke, M. Winter, *Nat. Energy.* **2018**, *3*, 267–278; d) J. W. Choi, D. Aurbach, *Nat. Rev. Mater.* **2016**, *1*, 1401826–1401841; e) P. Meister, H. Jia, J. Li, R. Kloepsch, M. Winter, T. Placke, *Chem. Mater.* **2016**, *28*, 7203–7217.
[5] A. F. Holleman, E. Wiberg, N. Wiberg, *Lehrbuch der anorganischen Chemie*, de Gruyter, Berlin, **2007**.
[6] E. A. Olivetti, G. Ceder, G. G. Gaustad, X. Fu, *Joule* **2017**, *1*, 229–243.
[7] a) P. Ge, M. Fouletier, *Solid State Ionics* **1988**, *28–30*, 1172–1175; b) I. A. Udod, H. B. Orman, V. K. Genchel, *Carbon* **1994**, *32*, 101–106; c) Y. Mizutani, T. Abe, K. Ikeda, E. Ihara, M. Asano, T. Harada, M. Inaba, Z. Ogumi, *Carbon* **1997**, *35*, 61–65; d) W. Luo, J. Wan, B. Ozdemir, W. Bao, Y. Chen, J. Dai, H. Lin, Y. Xu, F. Gu, V. Barone, *Nano Lett.* **2015**, *15*, 7671–7677; e) D. Pontiroli, M. Aramini, M. Gaboardi, M. Mazzani, A. Gorreri, M. Riccò, I. Margiolaki, D. Sheptyakov, *Carbon* **2013**, *51*, 143–147; f) C. God, B. Bitschnau, K. Kapper, C. Lenardt, M. Schmuck, F. Mautner, S. Koller, *RSC Adv.* **2017**, *7*, 14168–14175; g) M. S. Dresselhaus, G. Dresselhaus, *Adv. Phys.* **2002**, *51*, 1–186; h) J. O. Besenhard, M. Winter, *ChemPhysChem* **2002**, *3*, 155–159.
[8] a) Y. Marcus, *Pure Appl. Chem.* **1985**, *57*, 1129–1132; b) R. Wibowo, L. Aldous, S. E. W. Jones, R. G. Compton, *Chem. Phys. Lett.* **2010**, *492*, 276–280.
[9] S. Komaba, T. Hasegawa, M. Dahbi, K. Kubota, *Electrochem. Commun.* **2015**, *60*, 172–175.
[10] a) M. Winter, J. O. Besenhard in *Handbook of battery materials* (Ed.: J. O. Besenhard), Wiley-VCH, Weinheim, New York, **1999**, 383–418; b) M. Winter, K.-C. Moeller, J. O. Besenhard in *Lithium batteries. Science and technology* (Eds.: G.-A. Nazri, G. Pistoia), Springer, New York, NY, **2009**, 145–194.
[11] X. Wu, Y. Chen, Z. Xing, C. W. K. Lam, S.-S. Pang, W. Zhang, Z. Ju, *Adv. Energy Mater.* **2019**, *9*, 1900343–1900388.
[12] J. Liu, T. Yin, B. Tian, B. Zhang, C. Qian, Z. Wang, L. Zhang, P. Liang, Z. Chen, J. Yan, *Adv. Energy Mater.* **2019**, *9*, 1900579–1900589.
[13] T. Placke, A. Heckmann, R. Schmuch, P. Meister, K. Beltrop, M. Winter, *Joule* **2018**, *2*, 2528–2550.
[14] M. Wang, Y. Tang, *Adv. Energy Mater.* **2018**, *8*, 1703320–1703339.
[15] T. Ishihara, M. Koga, H. Matsumoto, M. Yoshio, *Electrochem. Solid-State Lett.* **2007**, *10*, A74–A76.
[16] T. Placke, O. Fromm, S. F. Lux, P. Bieker, S. Rothermel, H.-W. Meyer, S. Passerini, M. Winter, *J. Electrochem. Soc.* **2012**, *159*, A1755–A1765.
[17] a) T. Placke, P. Bieker, S. F. Lux, O. Fromm, H.-W. Meyer, S. Passerini, M. Winter, *Z. Phys. Chem.* **2012**, *226*, 391–407; b) J. A. Read, A. V. Cresce, M. H. Ervin, K. Xu, *Energy Environ. Sci.* **2014**, *7*, 617–620; c) T. Placke, G. Schmuelling, R. Kloepsch, P. Meister, O. Fromm, P. Hilbig, H.-W. Meyer, M. Winter, *Z. Anorg. Allg. Chem.* **2014**, *640*, 1996–2006.

[18] S. Rothermel, P. Meister, O. Fromm, J. Huesker, H. W. Meyer, M. Winter, T. Placke, *ECS Trans.* **2014**, *58*, 15–25.
[19] K. Beltrop, S. Beuker, A. Heckmann, M. Winter, T. Placke, *Energy Environ. Sci.* **2017**, *10*, 2090–2094.
[20] L. Fan, Q. Liu, S. Chen, K. Lin, Z. Xu, B. Lu, *Small* **2017**, *13*, 1701011–1701017.
[21] a) B. Ji, F. Zhang, X. Song, Y. Tang, *Adv. Mater.* **2017**, *29*, 1700519–1700525; b) B. Ji, F. Zhang, N. Wu, Y. Tang, *Adv. Energy Mater.* **2017**, *7*, 1700920–1700925.
[22] J. Wang, Y. Yamada, K. Sodeyama, C. H. Chiang, Y. Tateyama, A. Yamada, *Nat. Commun.* **2016**, *7*, 12032–12040.
[23] a) S.-K. Jeong, M. Inaba, Y. Iriyama, T. Abe, Z. Ogumi, *J. Electrochem. Soc.* **2003**, *6*, A13-A15; b) S.-K. Jeong, H.-Y. Seo, D.-H. Kim, H.-K. Han, J.-G. Kim, Y. B. Lee, Y. Iriyama, T. Abe, Z. Ogumi, *Electrochem. Commun.* **2008**, *10*, 635–638.
[24] Y. Yamada, M. Yaegashi, T. Abe, A. Yamada, *Chem. Commun.* **2013**, *49*, 11194–11196.
[25] Y. Yamada, K. Furukawa, K. Sodeyama, K. Kikuchi, M. Yaegashi, Y. Tateyama, A. Yamada, *J. Am. Chem. Soc.* **2014**, *136*, 5039–5046.
[26] Y. Yamada, K. Usui, C. H. Chiang, K. Kikuchi, K. Furukawa, A. Yamada, *ACS Appl. Mater. Interfaces* **2014**, *6*, 10892–10899.
[27] A. Heckmann, J. Thienenkamp, K. Beltrop, M. Winter, G. Brunklaus, T. Placke, *Electrochim. Acta* **2018**, *260*, 514–525.
[28] Y. Yamada, A. Yamada, *J. Electrochem. Soc.* **2015**, *162*, A2406–A2423.
[29] K. Sodeyama, Y. Yamada, K. Aikawa, A. Yamada, Y. Tateyama, *J. Phys. Chem. C* **2014**, *118*, 14091–14097.
[30] a) F. Chen, P. Howlett, M. Forsyth, *J. Phys. Chem. C* **2017**, *122*, 105–114; b) E. Flores, G. Åvall, S. Jeschke, P. Johansson, *Electrochim. Acta* **2017**, *233*, 134–141.
[31] Y. Yamada, A. Yamada, *Chem. Lett.* **2017**, *46*, 1056–1064.
[32] K. Matsumoto, K. Inoue, K. Nakahara, R. Yuge, T. Noguchi, K. Utsugi, *J. Power Sources* **2013**, *231*, 234–238.
[33] M. Nie, D. P. Abraham, D. M. Seo, Y. Chen, A. Bose, B. L. Lucht, *J. Phys. Chem. C* **2013**, *117*, 25381–25389.
[34] Q. Zhang, J. Pan, P. Lu, Z. Liu, M. W. Verbrugge, B. W. Sheldon, Y.-T. Cheng, Y. Qi, X. Xiao, *Nano Lett.* **2016**, *16*, 2011–2016.
[35] K. Xu, *Chem. Rev.* **2004**, *104*, 4303–4418.
[36] I. Cekic-Laskovic, N. von Aspern, L. Imholt, S. Kaymaksiz, K. Oldiges, B. R. Rad, M. Winter, *Top. Curr. Chem.* **2017**, *375*, 37–101.
[37] A. Heckmann, P. Meister, L.-Y. Kuo, M. Winter, P. Kaghazchi, T. Placke, *Electrochim. Acta* **2018**, *284*, 669–680.
[38] S. Miyoshi, H. Nagano, T. Fukuda, T. Kurihara, M. Watanabe, S. Ida, T. Ishihara, *J. Electrochem. Soc.* **2016**, *163*, A1206-A1213.
[39] J. Zhao, X. Zou, Y. Zhu, Y. Xu, C. Wang, *Adv. Funct. Mater.* **2016**, *26*, 8103–8110.
[40] Z. Jian, W. Luo, X. Ji, *J. Am. Chem. Soc.* **2015**, *137*, 11566–11569.
[41] K. Xu, *Chem. Rev.* **2014**, *114*, 11503–11618.
[42] M. Kerner, N. Plylahan, J. Scheers, P. Johansson, *Phys. Chem. Chem. Phys.* **2015**, *17*, 19569–19581.
[43] N. Xiao, W. D. McCulloch, Y. Wu, *J. Am. Chem. Soc.* **2017**, *139*, 9475–9478.
[44] Q. Zhang, J. Mao, W. K. Pang, T. Zheng, V. Sencadas, Y. Chen, Y. Liu, Z. Guo, *Adv. Energy Mater.* **2018**, *8*, 1703288–1703297.
[45] K. Beltrop, P. Meister, S. Klein, A. Heckmann, M. Grünebaum, H.-D. Wiemhöfer, M. Winter, T. Placke, *Electrochim. Acta* **2016**, *209*, 44–55.
[46] S.-D. Han, S.-H. Yun, O. Borodin, D. M. Seo, R. D. Sommer, V. G. Young, W. A. Henderson, *J. Phys. Chem. C* **2015**, *119*, 8492–8500.
[47] D. W. McOwen, D. M. Seo, O. Borodin, J. Vatamanu, P. D. Boyle, W. A. Henderson, *Energy Environ. Sci.* **2014**, *7*, 416–426.
[48] D. M. Seo, P. D. Boyle, R. D. Sommer, J. S. Daubert, O. Borodin, W. A. Henderson, *J. Phys. Chem. B* **2014**, *118*, 13601–13608.
[49] M. Beran, J. Příhoda, Z. Žák, M. Černík, *Polyhedron* **2006**, *25*, 1292–1298.
[50] A. V. Cresce, S. M. Russell, O. Borodin, J. A. Allen, M. A. Schroeder, M. Dai, J. Peng, M. P. Gobet, S. G. Greenbaum, R. E. Rogers, *Phys. Chem. Chem. Phys.* **2016**, *19*, 574–586.
[51] B. Ravikumar, M. Mynam, B. Rai, *J. Phys. Chem. C* **2018**, *122*, 8173–8181.
[52] a) J. Kasnatscheew, M. Börner, B. Streipert, P. Meister, R. Wagner, I. Cekic Laskovic, M. Winter, *J. Power Sources* **2017**, *362*, 278–282; b) E. Krämer, S. Passerini, M. Winter, *ECS Electrochem. Lett.* **2012**, *1*, C9-C11; c) E. Krämer, T. Schedlbauer, B. Hoffmann, L. Terborg, S. Nowak, H. J. Gores, S. Passerini, M. Winter, *J. Electrochem. Soc.* **2013**, *160*, A356–A360.
[53] B. Heidrich, A. Heckmann, K. Beltrop, M. Winter, T. Placke, *Energy Storage Mater.* **2019**, DOI: 10.1016/j.ensm.2019.05.031.
[54] S.-T. Myung, Y. Hitoshi, Y.-K. Sun, *J. Mater. Chem. A* **2011**, *21*, 9891–9911.
[55] P. Meister, X. Qi, R. Kloepsch, E. Krämer, B. Streipert, M. Winter, T. Placke, *ChemSusChem* **2017**, *10*, 804–814.
[56] C. Zhang, A. Yamazaki, J. Murai, J.-W. Park, T. Mandai, K. Ueno, K. Dokko, M. Watanabe, *J. Phys. Chem. C* **2014**, *118*, 17362–17373.
[57] T. Hosaka, K. Kubota, H. Kojima, S. Komaba, *Chem. Commun.* **2018**, *54*, 8387–8390.
[58] L. Fan, R. Ma, Q. Zhang, X. Jia, B. Lu, *Angew. Chem.* **2019**, *58*, 10500–10505.
[59] J. Ge, L. Fan, J. Wang, Q. Zhang, Z. Liu, E. Zhang, Q. Liu, X. Yu, B. Lu, *Adv. Energy Mater.* **2018**, *8*, 1801477–1801483.
[60] a) H. Yang, K. Kwon, T. M. Devine, J. W. Evans, *J. Electrochem. Soc.* **2000**, *147*, 4399–4407; b) S. S. Zhang, T. R. Jow, *J. Power Sources* **2002**, *109*, 458–464.
[61] A. Heckmann, M. Krott, B. Streipert, S. Uhlenbruck, M. Winter, T. Placke, *ChemPhysChem* **2017**, *18*, 156–163.
[62] M. Okoshi, Y. Yamada, S. Komaba, A. Yamada, H. Nakai, *J. Electrochem. Soc.* **2016**, *164*, A54-A60.
[63] a) Y. Liu, F. Fan, J. Wang, Y. Liu, H. Chen, K. L. Jungjohann, Y. Xu, Y. Zhu, D. Bigio, T. Zhu, *Nano Lett.* **2014**, *14*, 3445–3452; b) J. C. Pramudita, V. K. Peterson, J. A. Kimpton, N. Sharma, *Powder Diffr.* **2017**, *32*, S43–S48.
[64] a) N. Takenaka, T. Fujie, A. Bouibes, Y. Yamada, A. Yamada, M. Nagaoka, *J. Phys. Chem. C* **2018**, *122*, 2564–2571; b) V. Nilsson, R. Younesi, D. Brandell, K. Edström, P. Johansson, *J. Power Sources* **2018**, *384*, 334–341.
[65] K. V. Kravchyk, P. Bhauriyal, L. Piveteau, C. P. Guntlin, B. Pathak, M. V. Kovalenko, *Nat. Commun.* **2018**, *9*, 4469–4477.
[66] S. Wang, K. V. Kravchyk, A. N. Filippin, R. Widmer, A. N. Tiwari, S. Buecheler, M. I. Bodnarchuk, M. V. Kovalenko, *ACS Appl. Energy Mater.* **2019**, *2*, 974–978.
[67] M. Nie, B. L. Lucht, *J. Electrochem. Soc.* **2014**, *161*, A1001–A1006.
[68] V. Sharova, A. Moretti, T. Diemant, A. Varzi, R. J. Behm, S. Passerini, *J. Power Sources* **2018**, *375*, 43–52.
[69] S.-J. Kang, K. Park, S.-H. Park, H. Lee, *Electrochim. Acta* **2018**, *259*, 949–954.
[70] B. Philippe, R. Dedryvère, M. Gorgoi, H. Rensmo, D. Gonbeau, K. Edström, *J. Am. Chem. Soc.* **2013**, *135*, 9829–9842.
[71] D. Y. Wang, A. Xiao, L. Wells, J. R. Dahn, *J. Electrochem. Soc.* **2014**, *162*, A169–A175.
[72] M. Dahbi, F. Ghamouss, F. Tran-Van, D. Lemordant, M. Anouti, *J. Power Sources* **2011**, *196*, 9743–9750.
[73] T. Zhang, E. Paillard, *Front. Chem. Sci. Eng.* **2018**, *12*, 577–591.
[74] P. Zeng, Y. Han, X. Duan, G. Jia, L. Huang, Y. Chen, *Mater. Res. Bull.* **2017**, *95*, 61–70.
[75] G. G. Eshetu, T. Diemant, S. Grugeon, R. J. Behm, S. Laruelle, M. Armand, S. Passerini, *ACS Appl. Mater. Interfaces* **2016**, *8*, 16087–16100.
[76] J. Kasnatscheew, T. Placke, B. Streipert, S. Rothermel, R. Wagner, P. Meister, I. C. Laskovic, M. Winter, *J. Electrochem. Soc.* **2017**, *164*, A2479–A2486.
[77] a) W.-H. Li, Q.-L. Ning, X.-T. Xi, B.-H. Hou, J.-Z. Guo, Y. Yang, B. Chen, X.-L. Wu, *Adv. Mater.* **2019**, *31*, 1804766–1804773; b) X.-T. Xi, X. Feng, X.-J. Nie, B.-H. Hou, W.-H. Li, X. Yang, A.-B. Yang, W.-D. Sun, X.-L. Wu, *Chem. Commun.* **2019**, *55*, 8406–8409; c) X.-T. Xi, W.-H. Li, B.-H. Hou, Y. Yang, Z.-Y. Gu, X.-L. Wu, *ACS Appl. Energy Mater.* **2019**, *2*, 201–206.
[78] R. Nölle, K. Beltrop, F. Holtstiege, J. Kasnatscheew, T. Placke, M. Winter, *Mater. Today* **2019**, DOI: 10.1016/j.mattod.2019.07.002.

Manuscript received: July 27, 2019
Revised manuscript received: August 13, 2019
Accepted manuscript online: August 19, 2019
Version of record online: September 3, 2019